Theoretical and experimental differential cross sections for electron impact excitation of the electronic bands of furfural

D. B. Jones, R. F. C. Neves, M. C. A. Lopes, R. F. da Costa, M. T. do N. Varella, M. H. F. Bettega, M. A. P. Lima' , G. García, P. Limão-Vieira, and M. J. Brunger'

Citation: The Journal of Chemical Physics **144**, 124309 (2016); doi: 10.1063/1.4944615

View online: http://dx.doi.org/10.1063/1.4944615

View Table of Contents: http://aip.scitation.org/toc/jcp/144/12

Published by the American Institute of Physics

Theoretical and experimental differential cross sections for electron impact excitation of the electronic bands of furfural

D. B. Jones,[1] R. F. C. Neves,[2,3] M. C. A. Lopes,[3] R. F. da Costa,[4,5] M. T. do N. Varella,[6] M. H. F. Bettega,[7] M. A. P. Lima,[5,a)] G. García,[8] P. Limão-Vieira,[9] and M. J. Brunger[1,10,b)]
[1]*School of Chemical and Physical Sciences, Flinders University, GPO Box 2100, Adelaide, SA 5001, Australia*
[2]*Instituto Federal do Sul de Minas Gerais, Câmpus Poços de Caldas, Minas Gerais, Brazil*
[3]*Departamento de Física, UFJF, Juiz de Fora, Minas Gerais 36036-900, Brazil*
[4]*Centro de Ciências Naturais e Humanas, Universidade Federal do ABC, Santo André, São Paulo 09210-580, Brazil*
[5]*Instituto de Física "Gleb Wataghin," Universidade Estadual de Campinas, Campinas, São Paulo 13083-859, Brazil*
[6]*Instituto de Física, Universidade de São Paulo, CP 66318, 05315-970 São Paulo, Brazil*
[7]*Departamento de Física, Universidade Federal do Paraná, CP 19044, Curitiba, Paraná 81531-990, Brazil*
[8]*Instituto de Física Fundamental, CSIC, Serrano 113-bis, 28006 Madrid, Spain*
[9]*Laboratório de Colisões Atómicas e Moleculares, CEFITEC, Departamento de Física, Faculdade de Ciências e Tecnologia, Universidade NOVA de Lisboa, 2829-516 Caparica, Portugal*
[10]*Institute of Mathematical Sciences, University of Malaya, 50603 Kuala Lumpur, Malaysia*

(Received 12 January 2016; accepted 18 February 2016; published online 29 March 2016)

We report results from a joint experimental and theoretical investigation into electron scattering from the important industrial species furfural ($C_5H_4O_2$). Specifically, differential cross sections (DCSs) have been measured and calculated for the electron-impact excitation of the electronic states of $C_5H_4O_2$. The measurements were carried out at energies in the range 20–40 eV, and for scattered-electron angles between 10° and 90°. The energy resolution of those experiments was typically ~80 meV. Corresponding Schwinger multichannel method with pseudo-potential calculations, for energies between 6–50 eV and with and without Born-closure, were also performed for a sub-set of the excited electronic-states that were accessed in the measurements. Those calculations were undertaken at the static exchange plus polarisation-level using a minimum orbital basis for single configuration interaction (MOB-SCI) approach. Agreement between the measured and calculated DCSs was qualitatively quite good, although to obtain quantitative accord, the theory would need to incorporate even more channels into the MOB-SCI. The role of multichannel coupling on the computed electronic-state DCSs is also explored in some detail. [http://dx.doi.org/10.1063/1.4944615]

I. INTRODUCTION

In our recent investigations into the quantum chemical structure and electronic-state spectroscopy of furfural,[1] its ionisation dynamics[2] and its vibrational spectroscopy,[3] we made the case for furfural being identified as a key platform chemical[4,5] in the commercial realisation of bio-refineries.[6] We therefore do not repeat the detail of those arguments here, rather we reiterate briefly the following rationale. Furfural is solely produced through the thermochemical pre-treatment of biomass and so while it is desirable, from a commodity viewpoint, to increase the conversion efficiency of hemicellulose into furfural, its production within some bio-refineries is actually undesirable. This follows as it can inhibit enzymes responsible for up-conversion of pre-treated biomass.[7,8] As noted previously by us,[1] hybrid strategies represent a possible path forward to realising novel methods in biomass conversion,[9] with atmospheric pressure plasmas,[10,11] or electron-beam irradiation (EBI)[12,13] having been identified as alternative approaches for pre-treating biomass. Understanding, through modelling for instance, electron-driven and photochemical processes and reaction rates, with key structural analogues of biomass like furfural, is important in comprehending and possibly controlling the mechanisms that occur in plasma or EBI pre-treatments with a view of promoting or eliminating particular chemical pathways.

Furfural is a planar molecule that can exist in either a *trans*- or *cis*-conformation. The preferred furfural structure and its rotational barrier have been the subject of numerous investigations (see Refs. 14 and 15, and references therein), so it is now well established that in the gas phase, the *trans* conformer is preferred, and that the relative conformation populations are *trans* (79.5%) and *cis* (20.5%). We have previously shown, however, in the elastic scattering channel,[1,16] that the Schwinger Multichannel (SMC) results for the differential cross sections (DCSs) were, over a range of incident electron energies, very similar for the *trans*- and *cis*-conformers. Similarly, in our study of the ionisation dynamics in furfural,[2] distorted wave (DW) calculations for the triple differential cross sections of the *trans*- and *cis*-conformers,

a)Electronic mail: maplima@ifi.unicamp.br
b)Electronic mail: Michael.Brunger@flinders.edu.au

for both the HOMO and next highest occupied molecular orbital (NHOMO) and a range of kinematical conditions, were also very similar. Therefore, it is reasonable to undertake the computations for the *trans* conformer alone and make a valid comparison to the measured data whose furfural beam is constituted with the above conformational mixture. This is no moot point, calculating electronic-state DCSs is a very time consuming and computationally expensive task so that only having to do so for the *trans* conformer assists greatly in making the calculations more tractable.

Irrespective of our aim to provide reliable cross sections for plasma simulation studies, furfural possesses several intrinsic physico-chemical properties which, from our experience with other scattering systems,[17–25] are anticipated to play important roles in the collision dynamics. Specifically, furfural has a permanent dipole moment of magnitude ~3.46–3.57 D[26,27] and a significant average dipole polarisability of ~59.92 a_0^3.[28] We therefore also sought to investigate how those particular physico-chemical properties manifested themselves on the behaviour of the electronic-state DCSs of furfural, with particular interest in analysing their influence on the angular distributions. Aside from the previous results of our team on the scattering of electrons from furfural,[1–3,16] no other relevant scattering work appears to be currently available in the literature. Given the importance of furfural in many industries,[29] this sparsity of data is a little surprising but as a consequence, we believe the present theoretical and experimental electronic-state DCS efforts are original.

The structure of the remainder of this paper is as follows. In Sec. II, we describe our experimental methods and analysis procedures, while in Sec. III, details of our present computations can be found. Thereafter, in Sec. IV, our experimental and Schwinger multichannel method with pseudo-potentials (SMCPP) calculated DCSs are presented and discussed, before some conclusions from this study are given in Sec. V.

II. EXPERIMENTAL METHODS AND ANALYSIS

To determine absolute differential cross sections for electron impact excitation of the bands (Bands I-VI) of inelastic electronic-states in furfural,[1] we begin with measurements of electron energy loss spectra (EELS). Typical examples of some EELS from this investigation are given in Fig. 1, which also indicates the bands of electronic-states in furfural, below the first ionisation threshold, as classified in the work of Ferreira da Silva *et al.*[1] The present energy loss spectra were collected by an apparatus based at Flinders University, as originally described in Brunger and Teubner.[30] However, briefly, we note here that a monochromated electron beam with energies in the range 20–40 eV and a typical current of 1–6 nA was incident on an orthogonal beam of furfural (Sigma Aldrich; 99% assay) molecules. Furfural was not an easy target to work with, with our procedures for ensuring a stable beam being given in Jones *et al.*[3] Note that the furfural is introduced into the vacuum chamber through a variable leak valve, which is in turn coupled to a single channel capillary needle (molybdenum) of 0.7 mm inner diameter that acts as the molecular beam-forming device.

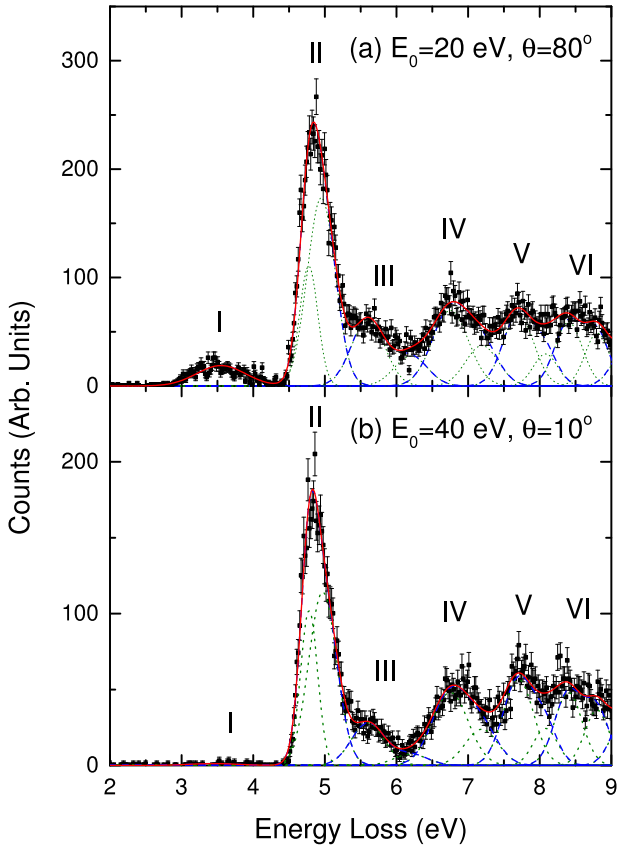

FIG. 1. Typical electron energy loss spectrum of furfural at (a) $E_0 = 20$ eV and $\theta = 80°$ and (b) $E_0 = 40$ eV and $\theta = 10°$. The overall spectral deconvolution fit is denoted by the solid red line, while the fits to the various Bands I–VI are also shown as dashed blue lines. The short-dashed green lines represent the individual Gaussian functions employed in the fit. Refer the work of Ferreira da Silva *et al.*[1] for further details on the assignments of Bands I–VI. Note that in each case, the elastic peak has been suppressed for clarity.

Under the stable beam conditions maintained during the EELS measurements, the furfural pressure in the vacuum chamber never exceeded 2×10^{-5} Torr in order to minimise any possible multiple scattering effects. The intersection of the electron and furfural beams defines a collision volume (interaction region), and those electrons which collided with the molecules and scattered at some angle θ, called the electron scattering angle, were energy analysed using a hemispherical selector before being detected with a channel electron multiplier. Note that the angular range of the present EELS was 10°–90°, while the angular resolution of the analyser is 2°. Further note that the overall instrumental energy resolution in these measurements was ~80 meV (FWHM), which was insufficient to resolve many of the electronic-states from one another.[1] Consequently, bands of excited electronic-states are reported here (see Fig. 1). EELSs were collected at each θ and incident electron energy (E_0 = 20, 30, or 40 eV) by recording the number of scattered electrons detected at each energy loss (E_L) value. The true electron count rate at each given E_L was recorded using a multichannel scaler synchronised to a linear voltage ramp that varied the detected energy loss between −0.2 and 9 eV. In this way, a given EELS is built up by continually scanning over the selected range of energy loss values, so that the effect of any variations in the incident electron current or target beam flux are minimised. In general, at each E_0 and θ, the EELS

TABLE I. Differential cross sections ($\times 10^{-16}$ cm^2/sr) for electron-impact excitation to the electronic-states in Band I ($E_L \sim 2.7$–4.3 eV) of furfural.

	$E_0 = 20$ eV			$E_0 = 30$ eV			$E_0 = 40$ eV		
Angle (deg)	Ratio	DCS	Uncert.	Ratio	DCS	Uncert.	Ratio	DCS	Uncert.
10							4.58×10^{-4}	2.21×10^{-2}	80
15				1.36×10^{-4}	4.21×10^{-3}	80	2.16×10^{-4}	5.51×10^{-3}	74
20	4.55×10^{-4}	9.22×10^{-3}	74	4.13×10^{-4}	6.12×10^{-3}	71	3.28×10^{-4}	3.80×10^{-3}	64
25							6.72×10^{-4}	3.57×10^{-3}	80
30	1.69×10^{-3}	9.02×10^{-3}	44	3.41×10^{-3}	1.13×10^{-2}	46	4.97×10^{-4}	1.40×10^{-3}	81
40	3.89×10^{-3}	8.47×10^{-3}	36	2.69×10^{-3}	3.88×10^{-3}	69	1.71×10^{-3}	2.16×10^{-3}	54
50	2.26×10^{-3}	2.43×10^{-3}	36	3.02×10^{-3}	2.62×10^{-3}	48	2.89×10^{-3}	2.72×10^{-3}	70
60	3.42×10^{-3}	3.06×10^{-3}	35	3.60×10^{-3}	2.74×10^{-3}	44	3.33×10^{-3}	2.49×10^{-3}	49
70	8.96×10^{-3}	7.01×10^{-3}	29	5.66×10^{-3}	3.34×10^{-3}	31	4.00×10^{-3}	2.05×10^{-3}	42
80	1.23×10^{-2}	9.02×10^{-3}	31	8.28×10^{-3}	4.14×10^{-3}	32	5.67×10^{-3}	2.26×10^{-3}	41
90	1.15×10^{-2}	7.23×10^{-3}	26	7.76×10^{-3}	3.57×10^{-3}	40	6.73×10^{-3}	2.77×10^{-3}	44

were measured 2–4 times to ensure that the measured inelastic to elastic ratios (see later) were reproducible.

In the work of Ferreira da Silva *et al.*,[1] we previously outlined the electronic-state spectroscopy of furfural and thus the basis of our spectral deconvolution approach. We, therefore, do not repeat that detail here. Instead, we simply note that the various EELS were deconvoluted, using a standard least-squares fitting procedure,[31] into contributions arising from each individual or unresolved combination of excited electronic-states. Either one or two Gaussian functions were employed to describe the spectral profiles for each resolvable inelastic feature (band) and the elastic scattering peak, with the positions and widths of the Gaussians being guided by the results of the quantum chemistry calculations in the work of Ferreira da Silva *et al.*[1] (see their Table I) and our experimental energy resolution. The detailed quantum chemistry calculations[1] lead us to believe that Band I (see Fig. 1), over $E_L \sim 2.7$–4.3 eV, is comprised of two experimentally unresolved electronic-states of triplet (^{3}A′, ^{3}A″) character and one symmetry-forbidden singlet (^{1}A″) state. Band II (see Fig. 1), over the E_L range ~4.3–5.3 eV, is also comprised of two optically forbidden triplet states (^{3}A′, ^{3}A′) and a strong dipole-allowed $\pi^* \leftarrow \pi$ ($\tilde{B}^1$A′ ← $\tilde{X}^1$A′) excitation. Hereafter the electronic-state spectroscopy becomes increasingly complicated, with the remaining bands often consisting of a combination of optically allowed and symmetry-forbidden singlet states, optically forbidden triplet states and in the case of Bands V and VI, Rydberg transitions.[1] Specifically though in Band III, with an energy loss range ~5.3–6.4 eV (see Fig. 1), we highlight an optically allowed ($\pi^* \leftarrow \pi$) transition of moderate strength, while for Band IV, E_L range ~6.4–7.4 eV, another ($\pi^* \leftarrow \pi$) transition dominates the photoabsorption spectrum consistent with the EELS in Fig. 1. In Band V (E_L range ~7.4–8.2 eV) and Band VI (E_L range ~8.2–9.0 eV), Ferreira da Silva *et al.*[1] found that there were a number of ($\pi^* \leftarrow \pi$) transitions that displayed strong mixing and also a rather large number of Rydberg excitations which they attempted to assign. It is interesting to note that neither the time dependent density functional theory (TDDFT) nor the full-single configuration interaction [FSCI] calculations of Ferreira da Silva *et al.*[1] were able to capture all the experimental optical oscillator strength for Bands IV–VI. This indicates limitations in the available quantum chemical descriptions of the electronic-states in those bands. Similarly, they also found that the FSCI calculation significantly overestimated the optical oscillator strength, compared to that of the experiment,[1] for the Band III electronic-states again reflecting a limitation with their description for those states. As the minimal orbital basis for single configuration interaction framework (MOB-SCI), to be

TABLE II. Differential cross sections ($\times 10^{-16}$ cm^2/sr) for electron-impact excitation to the electronic-states in Band II ($E_L \sim 4.3$–5.3 eV) of furfural.

	$E_0 = 20$ eV			$E_0 = 30$ eV			$E_0 = 40$ eV		
Angle (deg)	Ratio	DCS	Uncert.	Ratio	DCS	Uncert.	Ratio	DCS	Uncert.
10							2.94×10^{-2}	1.42×10^{0}	23
15				1.90×10^{-2}	5.88×10^{-1}	23	1.40×10^{-2}	3.57×10^{-1}	23
20	1.47×10^{-2}	2.99×10^{-1}	23	1.61×10^{-2}	2.38×10^{-1}	23	1.88×10^{-2}	2.18×10^{-1}	23
25							3.23×10^{-2}	1.72×10^{-1}	23
30	2.81×10^{-2}	1.50×10^{-1}	23	3.68×10^{-2}	1.22×10^{-1}	23	3.88×10^{-2}	1.09×10^{-1}	23
40	4.44×10^{-2}	9.65×10^{-2}	23	5.49×10^{-2}	7.93×10^{-2}	24	4.41×10^{-2}	5.59×10^{-2}	24
50	2.12×10^{-2}	2.27×10^{-2}	23	5.17×10^{-2}	4.47×10^{-2}	23	3.97×10^{-2}	3.74×10^{-2}	23
60	2.32×10^{-2}	2.08×10^{-2}	25	4.40×10^{-2}	3.35×10^{-2}	23	3.38×10^{-2}	2.52×10^{-2}	23
70	6.53×10^{-2}	5.11×10^{-2}	23	4.05×10^{-2}	2.39×10^{-2}	23	3.89×10^{-2}	1.99×10^{-2}	23
80	9.15×10^{-2}	6.71×10^{-2}	28	4.83×10^{-2}	2.41×10^{-2}	23	4.67×10^{-2}	1.86×10^{-2}	23
90	7.40×10^{-2}	4.66×10^{-2}	29	5.13×10^{-2}	2.36×10^{-2}	24	4.27×10^{-2}	1.76×10^{-2}	24

TABLE III. Differential cross sections ($\times 10^{-16}$ cm^2/sr) for electron-impact excitation to the electronic-states in Band III ($E_L \sim 5.3$–6.4 eV) of furfural.

	$E_0 = 20$ eV			$E_0 = 30$ eV			$E_0 = 40$ eV		
Angle (deg)	Ratio	DCS	Uncert.	Ratio	DCS	Uncert.	Ratio	DCS	Uncert.
10							6.91×10^{-3}	3.34×10^{-1}	27
15				5.14×10^{-3}	1.59×10^{-1}	24	4.02×10^{-3}	1.02×10^{-1}	27
20	2.89×10^{-3}	5.86×10^{-2}	29	4.83×10^{-3}	7.15×10^{-2}	24	5.43×10^{-3}	6.27×10^{-2}	26
25							9.28×10^{-3}	4.93×10^{-2}	26
30	6.43×10^{-3}	3.42×10^{-2}	26	1.51×10^{-2}	4.98×10^{-2}	25	1.21×10^{-2}	3.40×10^{-2}	28
40	1.70×10^{-2}	3.70×10^{-2}	24	1.79×10^{-2}	2.58×10^{-2}	28	1.46×10^{-2}	1.85×10^{-2}	27
50	4.12×10^{-3}	4.41×10^{-3}	30	1.68×10^{-2}	1.46×10^{-2}	24	1.40×10^{-2}	1.32×10^{-2}	28
60	5.99×10^{-3}	5.35×10^{-3}	29	1.50×10^{-2}	1.14×10^{-2}	25	1.25×10^{-2}	9.37×10^{-3}	27
70	2.34×10^{-2}	1.83×10^{-2}	25	1.64×10^{-2}	9.68×10^{-3}	24	1.50×10^{-2}	7.65×10^{-3}	25
80	3.68×10^{-2}	2.70×10^{-2}	33	2.08×10^{-2}	1.04×10^{-2}	24	1.89×10^{-2}	7.52×10^{-3}	26
90	3.03×10^{-2}	1.91×10^{-2}	33	2.15×10^{-2}	9.89×10^{-3}	26	1.86×10^{-2}	7.66×10^{-3}	29

used in the scattering computations (see Sec. III), is obtained with selected hole-particle pairs from the FSCI (the MOB-SCI contains up to 63 open electronic channels, the ground state plus 31 singlet (13 below $E_L = 10$ eV) and 31 triplet (17 below $E_L = 10$ eV) states), we restrict our reporting of the present SMCPP DCS results to Bands I and II although experimental DCSs are still reported for each of Bands I–VI. The amplitudes of the Gaussian functions representing Bands I–VI were now varied in our least-squares fitting procedure to provide the best fit to the measured spectra (see Fig. 1). The ratio (R) of the area under the fitting function for each ith inelastic band to that under the elastic feature, at each E_0 and θ, is simply related to the ratio of the differential cross sections (σ),

$$R_i(E_0,\theta) = \frac{\sigma_i(E_0,\theta)}{\sigma_0(E_0,\theta)}. \quad (1)$$

Note that Eq. (1) is only valid if the transmission efficiency of the analyser remains constant over the energy loss and angular range studied, or is at least well characterised. Following an approach similar to that of Allan,[32] and also influenced by the methodology at Sophia University,[33] an additional focusing lens (synchronised to the voltage ramp) was also employed to minimise variations in the angular transmission efficiency for electrons detected with different E_L. Our results suggest that the efficiency is unity, to within an uncertainty of 20%. The results for the present measured R_i, for each of Bands I–VI, are given, in the first columns of Tables I–VI, respectively.

It follows from Eq. (1) that the product $R_i \times \sigma_0$ gives the required electronic-state band differential cross sections provided the elastic DCSs (σ_0) are known. Those results, for each of Bands I–VI, can also be found in Tables I–VI. In this investigation, we have utilised the parallel version of our SMCPP computational approach,[34] that incorporates single-excitation configuration interaction techniques for the target description, for the elastic DCSs at 20 eV, 30 eV, and 40 eV. Note that no measured elastic DCSs for electron scattering from furfural are currently published, and given the challenges, we found in using furfural we are skeptical that any application of the relative flow technique[35] to attempt such measurements are likely. This follows as in using the relative flow method one necessarily cycles the target and standard gases throughout the measurements.[35] In our experience, the furfural pressure took some time to stabilise, making the duty cycle in a relative flow measurement with it as the target species highly problematic. The efficacy of using our SMCPP approach, to effect the normalisation of our R_i via Eq. (1), is discussed in detail elsewhere.[16] Here we simply note that similar to what we found in our recent investigation in phenol,[36] we believe the elastic SMCPP results[16] are a valid choice.

TABLE IV. Differential cross sections ($\times 10^{-16}$ cm^2/sr) for electron-impact excitation to the electronic-states in Band IV ($E_L \sim 6.4$–7.4 eV) of furfural.

	$E_0 = 20$ eV			$E_0 = 30$ eV			$E_0 = 40$ eV		
Angle (deg)	Ratio	DCS	Uncert.	Ratio	DCS	Uncert.	Ratio	DCS	Uncert.
10							1.43×10^{-2}	6.89×10^{-1}	24
15				1.20×10^{-2}	3.70×10^{-1}	23	1.00×10^{-2}	2.55×10^{-1}	23
20	4.78×10^{-3}	9.68×10^{-2}	26	1.04×10^{-2}	1.54×10^{-1}	23	1.03×10^{-2}	1.19×10^{-1}	24
25							1.42×10^{-2}	7.57×10^{-2}	24
30	7.37×10^{-3}	3.92×10^{-2}	28	1.88×10^{-2}	6.21×10^{-2}	25	2.01×10^{-2}	5.65×10^{-2}	25
40	1.94×10^{-2}	4.23×10^{-2}	24	3.04×10^{-2}	4.39×10^{-2}	25	2.67×10^{-2}	3.38×10^{-2}	25
50	3.35×10^{-3}	3.59×10^{-3}	34	3.04×10^{-2}	2.63×10^{-2}	23	2.32×10^{-2}	2.19×10^{-2}	25
60	4.70×10^{-3}	4.20×10^{-3}	32	2.44×10^{-2}	1.86×10^{-2}	24	1.74×10^{-2}	1.30×10^{-2}	25
70	2.16×10^{-2}	1.69×10^{-2}	25	2.17×10^{-2}	1.28×10^{-2}	24	2.18×10^{-2}	1.12×10^{-2}	24
80	4.35×10^{-2}	3.19×10^{-2}	39	3.02×10^{-2}	1.51×10^{-2}	23	2.93×10^{-2}	1.17×10^{-2}	24
90	3.47×10^{-2}	2.19×10^{-2}	38	3.29×10^{-2}	1.51×10^{-2}	24	2.74×10^{-2}	1.13×10^{-2}	26

TABLE V. Differential cross sections ($\times 10^{-16}$ cm^2/sr) for electron-impact excitation to the electronic-states in Band V ($E_L \sim 7.4$–8.2 eV) of furfural.

	$E_0 = 20$ eV			$E_0 = 30$ eV			$E_0 = 40$ eV		
Angle (deg)	Ratio	DCS	Uncert.	Ratio	DCS	Uncert.	Ratio	DCS	Uncert.
10							1.37×10^{-2}	6.63×10^{-1}	24
15				1.13×10^{-2}	3.48×10^{-1}	23	1.02×10^{-2}	2.61×10^{-1}	23
20	2.65×10^{-3}	5.37×10^{-2}	31	1.03×10^{-2}	1.52×10^{-1}	23	1.13×10^{-2}	1.31×10^{-1}	23
25							1.49×10^{-2}	7.93×10^{-2}	24
30	5.33×10^{-3}	2.84×10^{-2}	30	1.78×10^{-2}	5.89×10^{-2}	24	2.02×10^{-2}	5.67×10^{-2}	24
40	1.44×10^{-2}	3.14×10^{-2}	25	2.85×10^{-2}	4.11×10^{-2}	25	2.53×10^{-2}	3.20×10^{-2}	24
50	1.58×10^{-3}	1.69×10^{-3}	46	2.78×10^{-2}	2.41×10^{-2}	23	2.29×10^{-2}	2.16×10^{-2}	25
60	2.20×10^{-3}	1.97×10^{-3}	45	2.48×10^{-2}	1.89×10^{-2}	24	1.89×10^{-2}	1.41×10^{-2}	24
70	1.22×10^{-2}	9.52×10^{-3}	28	2.23×10^{-2}	1.32×10^{-2}	24	2.24×10^{-2}	1.15×10^{-2}	24
80	3.00×10^{-2}	2.20×10^{-2}	47	2.87×10^{-2}	1.44×10^{-2}	24	2.80×10^{-2}	1.12×10^{-2}	24
90	2.51×10^{-2}	1.58×10^{-2}	43	3.13×10^{-2}	1.44×10^{-2}	24	2.66×10^{-2}	1.10×10^{-2}	26

TABLE VI. Differential cross sections ($\times 10^{-16}$ cm^2/sr) for electron-impact excitation to the electronic-states in Band VI ($E_L \sim 8.2$–9.0 eV) of furfural.

	$E_0 = 20$ eV			$E_0 = 30$ eV			$E_0 = 40$ eV		
Angle (deg)	Ratio	DCS	Uncert.	Ratio	DCS	Uncert.	Ratio	DCS	Uncert.
10							1.26×10^{-2}	6.11×10^{-1}	24
15				1.16×10^{-2}	3.58×10^{-1}	23	9.92×10^{-3}	2.53×10^{-1}	23
20	1.85×10^{-3}	3.76×10^{-2}	32	1.06×10^{-2}	1.57×10^{-1}	23	1.23×10^{-2}	1.42×10^{-1}	23
25							1.64×10^{-2}	8.73×10^{-2}	23
30	4.63×10^{-3}	2.46×10^{-2}	29	2.04×10^{-2}	6.75×10^{-2}	24	2.32×10^{-2}	6.53×10^{-2}	24
40	1.58×10^{-2}	3.43×10^{-2}	25	3.45×10^{-2}	4.98×10^{-2}	26	3.02×10^{-2}	3.83×10^{-2}	25
50	1.92×10^{-3}	2.06×10^{-3}	45	3.42×10^{-2}	2.96×10^{-2}	23	2.77×10^{-2}	2.61×10^{-2}	24
60	2.25×10^{-3}	2.01×10^{-3}	58	2.99×10^{-2}	2.28×10^{-2}	23	2.40×10^{-2}	1.79×10^{-2}	24
70	1.01×10^{-2}	7.92×10^{-3}	31	2.68×10^{-2}	1.58×10^{-2}	23	2.79×10^{-2}	1.43×10^{-2}	24
80	3.04×10^{-2}	2.23×10^{-2}	48	3.66×10^{-2}	1.83×10^{-2}	23	3.74×10^{-2}	1.49×10^{-2}	23
90	2.47×10^{-2}	1.56×10^{-2}	45	4.14×10^{-2}	1.90×10^{-2}	23	3.56×10^{-2}	1.47×10^{-2}	25

Finally, we have paid some attention to the identification and quantification of all possible sources of experimental error in this study. Here, our error analysis combines in quadrature the statistical uncertainty associated with the deconvolution of our energy loss spectra and an uncertainty relating to the transmission efficiency of our analyser (20%). While the inherent error in our elastic SMCPP DCS computations is negligible, we have found from past experience[34] that it can often reproduce the experimental data to 10% or better between 20–40 eV. Hence a 10% error on the elastic DCSs has been incorporated into our analysis. The overall uncertainties on our inelastic furfural DCSs are found to be in the range 23%–81%, with the precise error depending on the energy, scattering angle and electronic-state band in question. Note that the upper limit on this error range is only for the Band I states at the more forward scattering angles, while the vast majority of the present measured inelastic DCSs have errors in the 23%–33% range. All the relevant percentage uncertainties are also tabulated in Tables I–VI.

III. SMCPP

In this paper, we have used the SMCPP,[37–39] in order to get theoretical cross sections for exciting the above discussed bands of furfural by electron impact. The theory was recently reviewed in Ref. 34, and here we only give a brief summary of the working expressions. In this method, the scattering amplitude is given by

$$f(\mathbf{k}_f, \mathbf{k}_i) = -\frac{1}{2\pi} \sum_{m,n} \langle S_{\mathbf{k}_f} | V | \chi_m \rangle (d^{-1})_{mn} \langle \chi_n | V | S_{\mathbf{k}_i} \rangle, \tag{2}$$

where

$$d_{mn} = \langle \chi_m | \left[\frac{\hat{H}}{N+1} - \frac{\hat{H}P + P\hat{H}}{2} + \frac{PV + VP}{2} - VG_P^{(+)}V \right] | \chi_n \rangle. \tag{3}$$

In the expressions above, P is a projector onto N_{open} energy-allowed target electronic channels, i.e.,

$$P = \sum_{\ell=1}^{N_{open}} |\Phi_\ell\rangle\langle\Phi_\ell|, \tag{4}$$

$G_P^{(+)}$ is the free-particle Green's function projected onto the P space, V is the projectile-target interaction potential, $\mathbf{k}_i$ ($\mathbf{k}_f$) is the incoming (outgoing) projectile wave vector, and $\hat{H} = E - H$ is the total energy (ground state energy plus kinetic energy of the incoming electron) minus the Hamiltonian of the $(N+1)$ electrons under the field of the fixed nuclei. The latter is given by $H = H_0 + V$, where H_0 describes the non-interacting electron-molecule system and $S_{\mathbf{k}}$ is a solution of H_0, namely, the product of a plane wave (projectile) and a target state Φ_ℓ (obtained within the scope of the single excitation configuration-interaction description). For the expansion of the variational scattering wave function, the method employs trial basis sets comprising $(N+1)$-particle configuration state functions (CSFs), denoted by χ_m, that are built from spin-adapted, anti-symmetrized products of target electronic states and projectile scattering orbitals. The open electronic collision channels are included in the P space and the dynamical response of the target electrons to the projectile field (correlation-polarisation effects) is accounted for through virtual excitations of the target. In this case, the CSFs are given by

$$|\chi_m\rangle = \mathcal{A}_{N+1}|\Phi_i(1,\ldots,N)\rangle \otimes |\varphi_j(N+1)\rangle, \tag{5}$$

where for $i > 0$, $|\Phi_i\rangle \equiv {}^{(2S+1)}(h_i \rightarrow p_i)$ is a singly excited state obtained by promoting one electron from a hole orbital (h_i) of the ground state $\Phi_0(1,\ldots,N)$ to a particle orbital (p_i), with either singlet ($S = 0$) or triplet ($S = 1$) spin coupling, although only $(N+1)$-electron configurations with total spin $S = 1/2$ (doublets) are actually taken into account. If we have N_{open} states in Eq. (4), this level of calculation is called an N_{open}-channel coupling scheme at the static-exchange-plus-polarisation (acronym is N_{open}ch-SEP) approximation.

In order to transform the scattering amplitude from the body-fixed frame (the reference frame best suited for carrying out the calculations) to the laboratory-fixed frame (the reference frame where the z-axis is aligned with the direction of incident wave vector, i.e., $\mathbf{k}_i = k_i\hat{\mathbf{z}}$), we expand $\mathbf{k}_f$ in terms of partial waves[34]

$$f(\mathbf{k}_f,\mathbf{k}_i) \equiv \langle\mathbf{k}_f|f|\mathbf{k}_i\rangle = \sum_{\ell=0}^{\ell_{max}} \sum_{m=-\ell}^{\ell} \langle\mathbf{k}_f|\ell m\rangle f(\ell m,\mathbf{k}_i), \tag{6}$$

where $\langle\mathbf{k}_f|\ell m\rangle$ is a spherical harmonic that can be easily converted from the body- to the laboratory-frame and $f(\ell m,\mathbf{k}_i) = \langle\ell m|f|\mathbf{k}_i\rangle$ can be understood as the scattering amplitude of an electron entering the interaction region in a plane-wave $|\mathbf{k}_i\rangle$ and leaving it in a partial wave $|\ell m\rangle$. Although not shown here, all SMCPP differential cross sections in this paper, over the entire energy range (5-50 eV), are numerically converged with $\ell_{max} = 10$ (except for 50 eV that demands $\ell_{max} = 13$), if combined with a quadrature point distribution, using a 26 Gauss-Legendre scheme for $0 \le \theta_i \le \pi$ and 52 points for $0 \le \phi_i \le 2\pi$, to describe $\mathbf{k}_i(\theta_i,\phi_i)$ in spherical coordinates. Although we have contributions from high partial waves in the scattering orbitals due to the multi-centre expansion, we only employ Cartesian Gaussians (CG) of s, p, and d types on the oxygen atom and on each center for the carbon atoms. On the hydrogen atoms, we have only CG functions of s and p type. As discussed in our previous applications,[34] this makes the description of the high partial waves more difficult but sufficient to obtain good convergence in the elastic differential cross sections.[16] We have also used pseudopotentials for the carbon and oxygen atoms. This strategy allows a reduction in the number of Cartesian Gaussian functions, since it is not necessary to consider those involved in the description of all 1s orbitals of these atoms.

For some cases (elastic and dipole-allowed singlet transitions) a Born-closure scheme was used following the same strategy as described in Ref. 34. This closure is obtained from the expression

$$\begin{aligned} f_{\mathrm{LAB}}^{\mathrm{closure}}(\mathbf{k}_f,\mathbf{k}_i) = {} & f_{\mathrm{LAB}}^{\mathrm{FBA}}(\mathbf{k}_f,\mathbf{k}_i) \\ & + \sum_{\ell=0}^{\ell_{max}} \sum_{m=-\ell}^{\ell} \left(f_{\mathrm{LAB}}(\ell m,\mathbf{k}_i) - f_{\mathrm{LAB}}^{\mathrm{FBA}}(\ell m,\mathbf{k}_i)\right) \\ & \times Y_{\ell m}^*(\mathbf{k}_f), \end{aligned} \tag{7}$$

where $f_{\mathrm{LAB}}^{\mathrm{FBA}}$ is the scattering amplitude for the permanent dipole moment potential for the elastic process or for the dipole transition potential for inelastic dipole-allowed processes. Both are obtained in the first Born approximation, in a closed form in the laboratory-frame. The amplitude $f_{\mathrm{LAB}}(\ell m,\mathbf{k}_i)$ is just the $f(\ell m,\mathbf{k}_i)$ of Eq. (6) transformed to this frame.

A. Description of the electronic states of furfural for the SMCPP application

As discussed, in more detail, in our paper about multichannel effects on the elastic scattering of furfural by electron impact,[16] the ground state of the furfural *trans* conformation was obtained in the Hartree-Fock approximation, using 241 CG functions (ns, np, nd on each C and O atom and ns, np on each H). We first ran a FSCI which gave 4014 states, with 32 (53) of them below 9 eV (10 eV) (from the ground state). Using a mixture of hole orbitals, we obtained a set of improved virtual orbitals capable of reproducing 26 below 9 eV (30 below 10 eV) of those states using only 31 hole-particle pairs. This procedure defined the MOB-SCI[38] of the present application. The 31 hole-particle pairs give rise to 31 triplets and 31 singlets states (see Table I in the work of Ferreira da Silva *et al.*[1]). In this description, 31 electronic states are open at 10 eV (31ch-SEP approximation), 53 electronic channels are open at 20 eV (53ch-SEP approximation), and all 63 electronic channels are open at 30 and 40 eV (63ch-no additional closed channels for SEP). As in the phenol application[24,36] of the SMCPP method, we discuss the convergence of the electronic excitation cross sections with respect to the number of open channels in the accompanying elastic paper.[16] Here, we only present figures (discussed in Sec. IV) showing the convergence trend for a few energies, by summing up the states involved in the first 2 bands. The phenol case had a maximum number of 33 open electronic states against the present

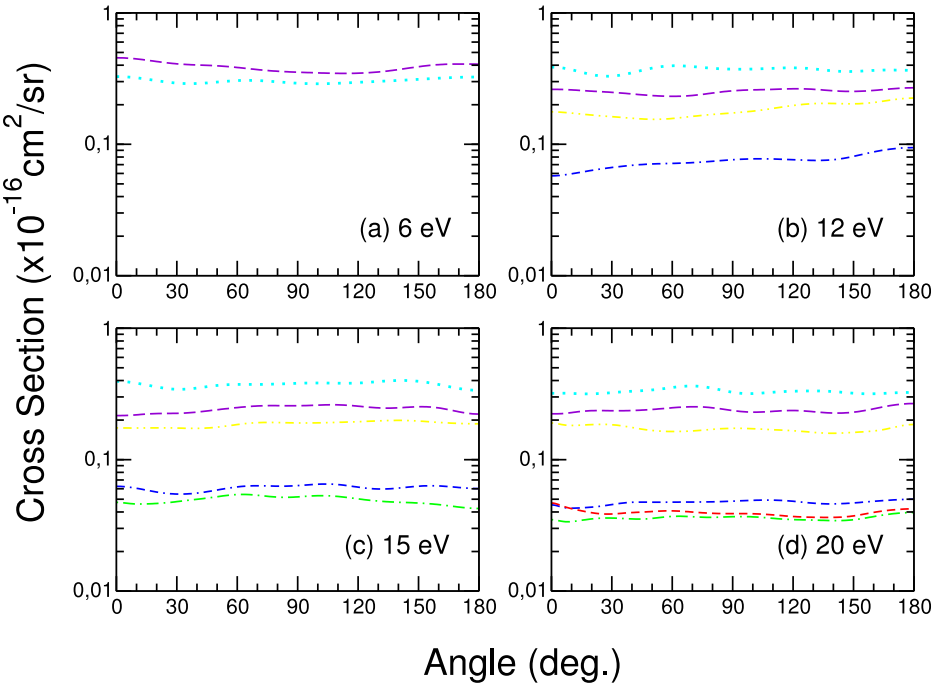

FIG. 2. Present SMCPP-SEP Band I electronic-state DCSs ($\times 10^{-16}$ cm^2/sr) at (a) 6 eV, (b) 12 eV, (c) 15 eV, and (d) 20 eV. Results are presented for 4, 6, 7, 31, 53, and 57 open channels, in each case for the outgoing electrons propagating out in partial waves up to $L = 13$ and including Born-closure. Please note our colour coding of 57 open channels (red-dashed line), 53 open channels (green long-dashed line), 31 open channels (blue-dash-dash-dotted line), 7 open channels (yellow dashed-dot-dotted line), 6 open channels (violet long-dashed line), and 4 open channels (cyan dotted line). See text for further details.

application with the projector P containing 63 electronic states for furfural. The present study is our most sophisticated (with the largest channel coupling) application of the SMCPP method. Although promising, it is important to point out that the present FSCI calculation,[1] with 241 CG functions, generated 32 electronic excited states below 9 eV, 53 below 10 eV, 102 below 12 eV, 263 below 15 eV, and 688 excited states below 20 eV. This high density molecular spectra, due to a combination of high density Rydberg states, increases as we augment the CG basis. Our MOB-SCI calculation includes most of the states (26 of the 32 FSCI states) below 9 eV but the computationally needed truncation generated important convergence consequences, as we will discuss in Sec. IV. Although not accounted for in the scattering calculation, the present Hartree-Fock approximation for the ground state of furfural shows the first 3 ionisation potentials (Koopman's theorem) at 9.2, 11.4 and 12.0 eV, respectively. Thus our MOB-SCI calculation is almost the complete calculation using all open channels up to 9 eV. Note, however, that a "complete" calculation using all possible open channels up to 12 eV would have the ground state plus 102 discrete excited states plus 3 ionisation channels.

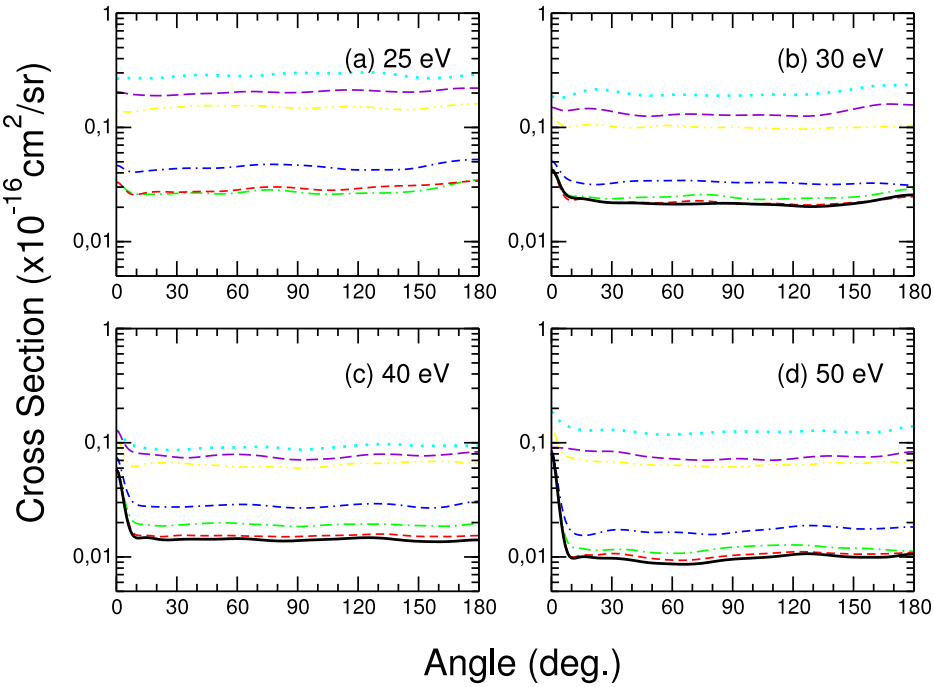

FIG. 3. Present SMCPP-SEP Band I electronic-state DCSs ($\times 10^{-16}$ cm^2/sr) at (a) 25 eV, (b) 30 eV, (c) 40 eV, and (d) 50 eV. Results are presented for 4, 6, 7, 31, 53, 57, and 63 open channels, in each case for the outgoing electrons propagating out in partial waves up to $L = 13$ and including Born-closure. Please note our colour coding of 63 open channels (black solid line), 57 open channels (red-dashed line), 53 open channels (green long-dashed line), 31 open channels (blue-dash-dash-dotted line), 7 open channels (yellow dashed-dot-dotted line), 6 open channels (violet long-dashed line), and 4 open channels (cyan dotted line). See text for further details.

IV. RESULTS AND DISCUSSION

In Figs. 2–5 we present our Bands I and II SMCPP-SEP results, for the cases of 4, 6, 7, 31, 53, 57, and 63 open electronic channels in our MOB-SCI framework and in each case for the incident electrons arriving as plane waves and exiting as spherical waves up to $L_{max} = 13$. Born-closure is applied throughout. Specifically, in Fig. 2 we plot our lower-energy Band I computational results for (a) 6 eV, (b) 12 eV, (c) 15 eV, and (d) 20 eV while in Fig. 3 we present our higher-energy results for (a) 25 eV, (b) 30 eV, (c) 40 eV, and (d) 50 eV. Similarly, in Fig. 4 we show our lower-energy Band II SMCPP-SEP calculations at (a) 12 eV, (b) 15 eV, and (c) 20 eV while in Fig. 5 we plot our higher-energy Band II results again at (a) 25 eV, (b) 30 eV, (c) 40 eV, and (d) 50 eV. As noted earlier in Sec. III, all the SMCPP-SEP results we present are converged with respect to the outgoing angular momentum, as defined in Eqs. (6) and (7). In Tables I–VI we provide the current measured differential cross sections for electron-impact excitation of the Bands I–VI (see Fig. 1) electronic states in furfural. Also shown in those tables are the associated overall percentage errors on the DCSs, which are reported to the one standard deviation level. Those data are also plotted for (a) 20 eV, (b) 30 eV, and (c) 40 eV in Fig. 6 for Band I, Fig. 7 for Band II and Fig. 8 for Bands III–VI. Additionally, in Figs. 6 and 7, we plot our most accurate (or physical) SMCPP-SEP results (57 open channels at 20 eV with 31 channels below $E_L = 10$ eV, and 63 open channels at 30 eV and 40 eV again with 31 channels below $E_L = 10$ eV), both with and without Born-closure, to enable a comparison between our present experimental and theoretical DCSs.

Let us now consider our theoretical results for Band I in more detail. It is apparent from Figs. 2 and 3 that as we increase the number of open channels into our SMCPP-SEP calculations, irrespective of the incident electron energy, the magnitude of the DCSs generally drops. Indeed, in going from the 4 open-channels to the 57 or 63 open-channels results, the DCS magnitude can decrease by an order of magnitude or more. This is an excellent illustration of what we refer to as multichannel coupling effects.[24,34] Probably the only exception to this general statement appears to be at 6 eV [Fig. 2(a)], where the 6-channels DCS is actually a little stronger in magnitude than that for the 4-channels case. However this is not an uncommon situation, having previously been seen by us in our phenol study.[24] Conversely, by increasing the number of open channels in the SMCPP-SEP computations we find that the angular distribution or shape of the DCSs do not significantly change. Indeed at energies up to about 25 eV the theoretical angular distributions are largely quasi-isotropic. This observation is not too surprising as Band I, as we noted previously, is comprised of two triplet and one symmetry-forbidden singlet state, so that its population mechanism will largely be determined by the electron exchange interaction whose typical angular distribution is consistent with those we find in Figs. 2 and 3(a). Only at 30 eV, 40 eV, and 50 eV do we see the effect of Born-closure, at the more forward scattered electron angles, on their angular distributions. This contribution is due to the excited singlet state in Band I, and is consistent with the strong permanent dipole moment

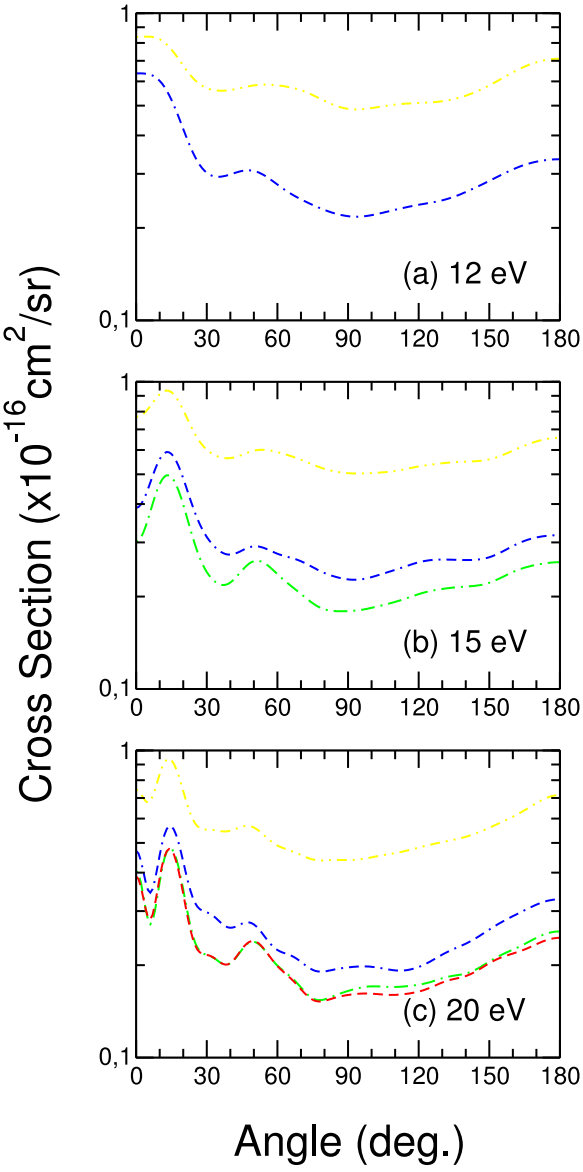

FIG. 4. Present SMCPP-SEP Band II electronic-state DCSs ($\times 10^{-16}$ cm^2/sr) at (a) 12 eV, (b) 15 eV, and (c) 20 eV. Results are presented for 7, 31, 53, and 57 open channels, in each case for the outgoing electrons propagating out in partial waves up to $L = 13$ and including Born-closure. Please note our colour coding of 57 open channels (red-dashed line), 53 open channels (green long-dashed line), 31 open channels (blue-dash-dash-dotted line), and 7 open channels (yellow dashed-dot-dotted line). See text for further details.

that furfural possesses.[26,27] If we now compare our Band I experimental data (see Table I and Fig. 6) to our most exact SMCPP-SEP results, incorporating 57 open channels at 20 eV and 63 open channels at 30 eV and 40 eV, we find an excellent qualitative level of accord between them with the experimental angular distributions also being quasi-isotropic in form. There is, however, a mismatch of about a factor of 5 in their absolute magnitude (the theory is larger), which we believe, at least in part, reflects our being restricted to a MOB-SCI framework in order to make these computationally expensive calculations tractable. In other words, if we could increase further the number of open channels in the target description we would, on the basis of the results in Figs. 2 and 3, anticipate this disparity in the absolute magnitude

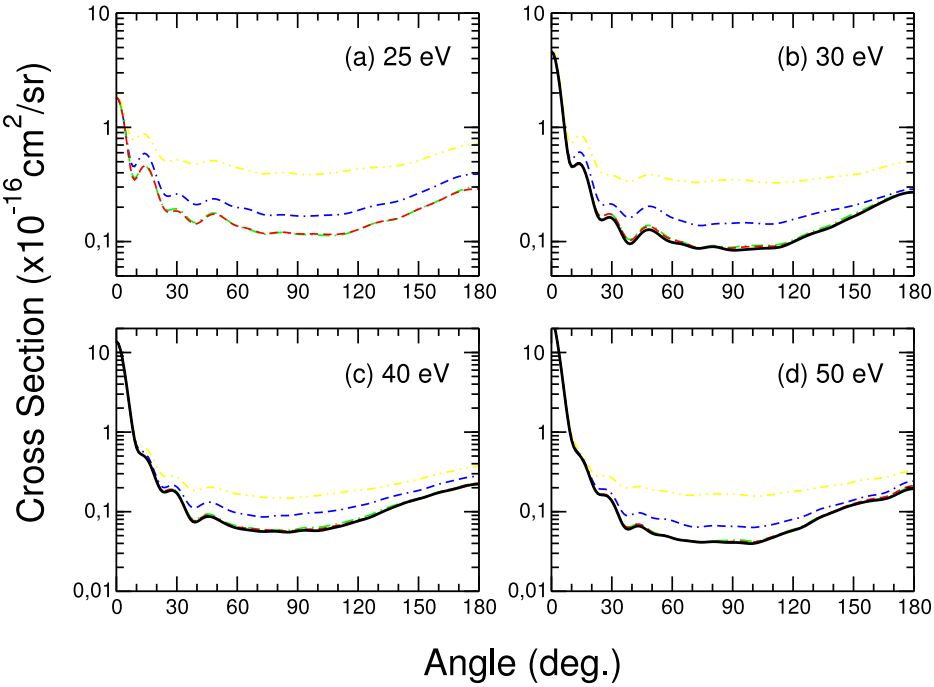

FIG. 5. Present SMCPP-SEP Band II electronic-state DCSs ($\times 10^{-16}$ cm^2/sr) at (a) 25 eV, (b) 30 eV, (c) 40 eV, and (d) 50 eV. Results are presented for 7, 31, 53, 57, and 63 open channels, in each case for the outgoing electrons propagating out in partial waves up to $L = 13$ and including Born-closure. Please note our colour coding of 63 open channels (black solid line), 57 open channels (red-dashed line), 53 open channels (green long-dashed line), 31 open channels (blue-dash-dash-dotted line), and 7 open channels (yellow dashed-dot-dotted line). See text for further details.

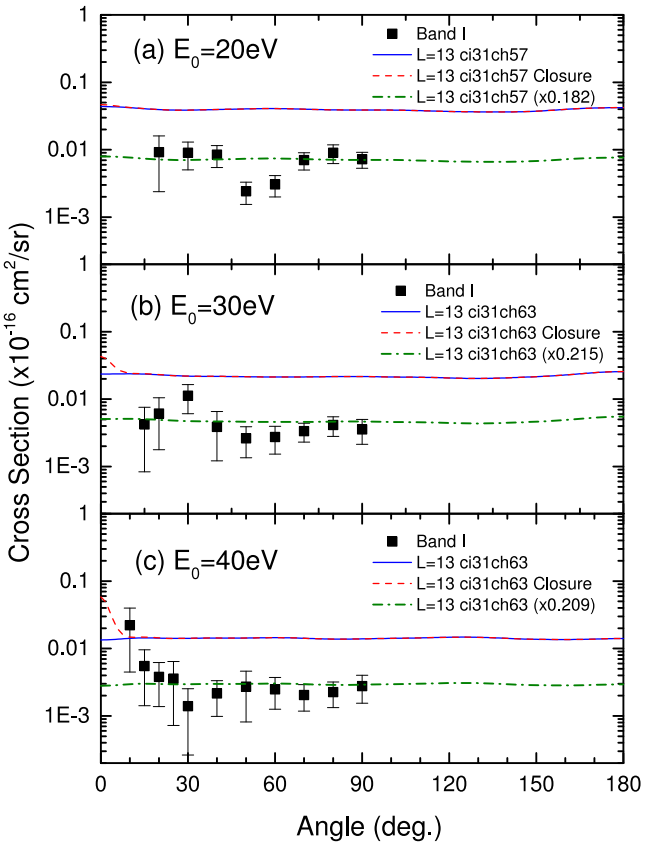

FIG. 6. Present DCSs ($\times 10^{-16}$ cm^2/sr) for electron impact excitation of the Band I electronic-states in furfural at (a) 20 eV, (b) 30 eV and (c) 40 eV. The measured data (■) are compared against our most accurate SMCPP-SEP calculations, both with (– – –) and without (—) Born-closure, and against the SMCPP-SEP results (no Born-closure) scaled to give best agreement with the measured data (– · – · –). See legend in figure and text for further details.

to lessen so that even better agreement would be achieved. However, it is worth noting from Figs. 2 and 3 that the rate of decrease in magnitude of the calculated DCSs is seen to decrease markedly in going from 31 to 53 open channels and then from 53 to 57 open channels and finally from 57 to 63 open channels. This suggests we would need to incorporate a quite significant further number of discrete open channels in the target description in order to obtain quantitative agreement between our measured and calculated results. On the other hand, the present Green's function in our SMC approach is not prepared for ionisation. In order to approximately mimic the inclusion of the effect of the target ionisation, we would need to include very diffuse Cartesian Gaussians and make excitations to them. Currently, however, our computer codes are not prepared to use very diffuse functions in our calculations because this type of diffuse function brings numerical problems in the matrix inversion using the SMC method. Note that in principle we know how to incorporate the diffuse functions, and have strategies to deal with any numerical problems encountered in doing so. But this is a non-trivial development and would come with some computational cost. Indeed perhaps a better way forward would be to account for the ion-states as competing channels through the use of an optical potential, such as employed for atomic targets by García and colleagues.[40] Nonetheless if we were to create flux competition between the continuum and the bound open channels in our computations then we would expect the magnitude of the theoretical Band I DCSs to decrease, perhaps significantly, and become in better accord with our measured data. Evidence in support of this assertion, for an atomic scattering system, in this case between measured neon electronic-state data from Sophia University and corresponding B-Spline R-matrix calculations from Drake University[41,42] (and references therein), is certainly available in the literature. However, we reiterate, it is not only the ionisation channels that are missing in our current

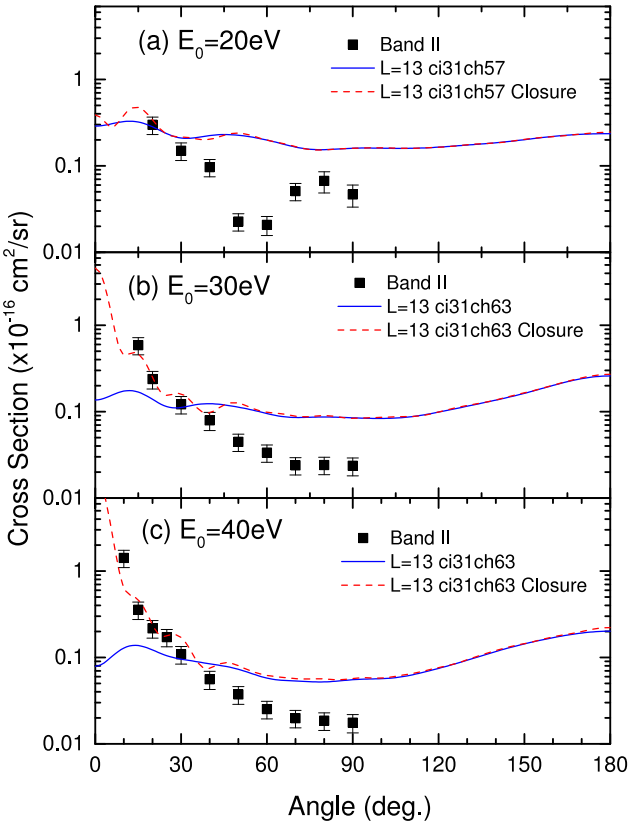

FIG. 7. Present DCSs ($\times 10^{-16}$ cm^2/sr) for electron impact excitation of the Band II electronic states in furfural at (a) 20 eV, (b) 30 eV, and (c) 40 eV. The measured data (■) are compared against our most accurate SMCPP-SEP calculations, both with (– – –) and without (—) Born-closure. See legend in figure and text for further details.

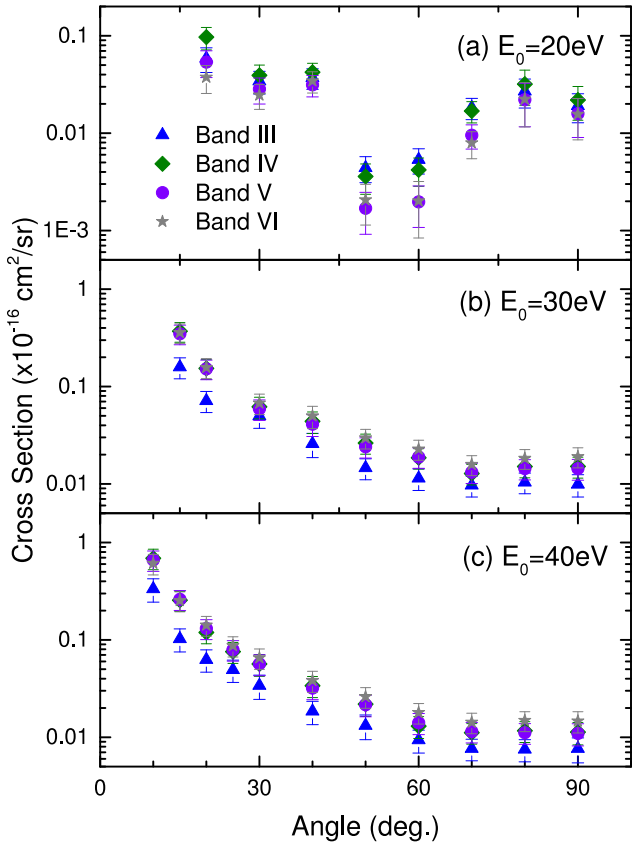

FIG. 8. Present DCSs ($\times 10^{-16}$ cm^2/sr) for electron impact excitation of the Bands III–VI electronic states in furfural at (a) 20 eV, (b) 30 eV, and (c) 40 eV. The measured data for Band III (▲), Band IV (◆), Band V (●) and Band VI (★) are shown. See legend in figure and text for further details.

computations. The missing discrete electronic (bound) states above ~9 eV may also be important to account for, in order to achieve quantitative agreement between theory and experiment. Their thresholds are near those for the ions-states and they all will compete for flux. One practical way to deal with this might be to treat all the bound states between 9–12 eV as being degenerate (therefore saving on a lot of integral calculations), in the manner detailed by da Costa *et al.*,[34] and this is a computational programming development that is currently in progress.

Considering now our Band II theoretical results in Figs. 4 and 5, we find again the important role played by multichannel coupling effects[34] in determining the magnitudes of the DCSs. As noted previously, Band II is comprised of two ^{3}A′ electronic-states and a strong dipole-allowed ^{1}A′ electronic-state. The contributions of these states, to the measured angular distributions for Band II, can be gleaned from Figs. 4 and 5. In particular, in Fig. 5 we see the increasing forward peaked nature of the angular distributions, as E_0 is increased, reflecting the importance of the strong permanent dipole moment of furfural on the $\pi^* \leftarrow \pi$ optically allowed transition to the ^{1}A′ electronic-state. The importance of describing the effect of the dipole moment, on the scattering dynamics, is perhaps best illustrated in Figs. 7(b) and 7(c) where we find quantitative agreement between our measured and calculated Band II data, for scattered electron angles less than about 45° and at E_0 = 30 eV and 40 eV, when Born-closure is allowed for. At scattered electron angles greater than 45°, the magnitude of the SMCPP-SEP DCSs is uniformly larger than those of the measured data although the shape agreement remains quite good. We would again anticipate that this level of agreement, at middle angles, would quantitatively improve if further open channels were to be able to be incorporated into the target description and if coupling of the discrete inelastic channels to the continuum were also possible. Nonetheless, given the complexity of these SMCPP-SEP calculations, the level of accord we find between our measurements and computations here is really quite heartening.

Finally, in Fig. 8 and Tables III–VI, we present our experimental DCSs for Bands III–VI and at the incident electron energies of 20 eV, 30 eV, and 40 eV. As Bands III–VI are all comprised of a mixture of triplet, dipole-allowed singlet, and symmetry-forbidden singlet excitations,[1] as well as Rydberg transitions in the case of Bands IV–VI, it is perhaps not (*a posteriori*) surprising to find that their angular distributions are all remarkably similar at each E_0. Indeed, to within the measurement uncertainties, the shapes of the DCSs for each of Bands III–VI are virtually identical. Band III is seen to have (see Fig. 8), particularly at 30 eV and 40 eV, a somewhat smaller magnitude DCS but this might be understood in terms of its smaller density of states compared to Bands IV–VI including an absence of Rydberg transitions.[1] In terms of general trends, we find the DCSs for each of Bands III–VI become increasingly forward peaked (i.e., as

you go to smaller θ) in magnitude as E_0 increases. This again, we believe, reflects the important role played by the dipole properties (i.e., the dipole moment and dipole polarisability) of the target furfural molecules on the collisional behaviour of the incident electrons.

Please note that although we give ranges of energy loss (E_L) values for the Bands I-VI of this investigation,[1] in terms of the threshold energies to be used in any possible modelling studies (for each band), it is the minimum E_L for each band that corresponds to the relevant threshold energy.

V. CONCLUSIONS

We have reported differential cross section results from SMCPP-SEP calculations and experimental measurements for electron impact excitation of bands of discrete electronic-states in furfural. The theoretical results were provided for the Bands I and II electronic-states, while the experimental data encompassed the Bands I–VI electronic-states (see Fig. 1). The importance of multichannel coupling, on the description of the electron–furfural scattering dynamics, was clearly established as a part of this study. Very good qualitative (and some quantitative) accord was found between our calculated and measured Bands I and II differential cross sections, with the observed magnitude discrepancies possibly being resolved by including more open channels in the target description and/or allowing for flux competition between the discrete channels and the continuum. However, the difficulty of instituting the latter suggestion, within an SMC approach, should not be underestimated. Finally we note that the present study, along with our earlier work on furfural,[1–3] takes us a little closer to being able to put together a database that might be used in modelling atmospheric pressure plasmas in which furfural is a constituent.

ACKNOWLEDGMENTS

R.F.C.N. thanks CNPq (Brazil) and the Science Without Borders Programme for opportunities to study abroad. D.B.J. thanks the Australian Research Council (ARC) for financial support provided through a Discovery Early Career Research Award, while M.J.B. also thanks the ARC for their support. M.J.B. and M.C.A.L. acknowledge the Brazilian agencies CNPq and FAPEMIG. P.L.-V. acknowledges the Portuguese Foundation for Science and Technology (FCT-MEC) through Grant Nos. PTDC/FIS-ATO/1832/2012 and UIO/FIS/00068/2013. G.G. acknowledges partial financial support from the Spanish Ministry MINECO (Project No. FIS2012-31230) and the European Union COST Action No. CM1301 (CELINA). Finally, R.F.d.C., M.T.d.N.V., M.H.F.B., and M.A.P.L. acknowledge support from the Brazilian agency CNPq and M.T.d.N.V. also thanks FAPESP.

[1]F. Ferreira da Silva, E. Lange, P. Limão-Vieira, N. C. Jones, S. V. Hoffmann, M.-J. Hubin-Franskin, J. Delwiche, M. J. Brunger, R. F. C. Neves, M. C. A. Lopes, E. M. de Oliveira, R. F. da Costa, M. T. do N. Varella, M. H. F. Bettega, F. Blanco, G. García, M. A. P. Lima, and D. B. Jones, J. Chem. Phys. **143**, 144308 (2015).
[2]D. B. Jones, E. Ali, K. L. Nixon, P. Limão-Vieira, M.-J. Hubin-Franskin, J. Delwiche, C. G. Ning, J. Colgan, A. J. Murray, D. H. Madison, and M. J. Brunger, J. Chem. Phys. **143**, 184310 (2015).
[3]D. B. Jones, R. F. C. Neves, M. C. A. Lopes, R. F. da Costa, M. T. do N. Varella, M. H. F. Bettega, M. A. P. Lima, G. García, F. Blanco, and M. J. Brunger, J. Chem. Phys. **143**, 224304 (2015).
[4]H. Gomez Bernal, L. Bornazzami, and A. M. Raspolli Galletti, Green Chem. **16**, 3734 (2014).
[5]J.-P. Lange, E. van der Heide, J. van Buijtenen, and R. Price, ChemSusChem **5**, 150 (2012).
[6]A. J. Ragauskas, C. K. Williams, B. H. Davison, G. Britovsek, J. Cairney, C. A. Eckert, W. J. Frederick, J. P. Hallett, D. J. Leak, C. L. Liotta, J. R. Mielenz, R. Murphy, R. Templer, and T. Tschaplinski, Science **311**, 484 (2006).
[7]J. D. Keating, C. Panganibon, and S. D. Mansfield, Biotechnol. Bioeng. **93**, 1196 (2006).
[8]P. Pienkos and M. Zhang, Cellulose **16**, 743 (2009).
[9]L. D. Schmidt and P. J. Danenhaver, Nature **447**, 914 (2007).
[10]J. Amorim, C. Oliveira, J. A. Souza-Corrêa, and M. A. Ridenti, Plasma Processes Polym. **10**, 670 (2013).
[11]N. Schultz-Jensen, F. Leipold, H. Bindslev, and A. Thomsen, Appl. Biochem. Biotechnol. **163**, 558 (2011).
[12]J. S. Bak, J. K. Ko, Y. H. Han, B. C. Lee, I.-G. Choi, and K. H. Kim, Bioresour. Technol. **100**, 1285 (2009).
[13]A. W. Khan, J. P. Labrie, and J. McKeown, Biotechnol. Bioeng. **28**, 1449 (1986).
[14]K. K. Baldridge, V. Jonas, and A. D. Bain, J. Chem. Phys. **113**, 7519 (2000).
[15]T. S. Little, J. Qiu, and J. R. Durig, Spectrochim. Acta, Part A **45**, 789 (1989).
[16]R. F. da Costa, M. T. do N. Varella, M. H. F. Bettega, R. F. C. Neves, M. C. A. Lopes, F. Blanco, G. García, D. B. Jones, M. J. Brunger, and M. A. P. Lima, J. Chem. Phys. **144**, 124310 (2016).
[17]T. P. T. Do, M. Leung, M. Fuss, G. Garcia, F. Blanco, K. Ratnavelu, and M. J. Brunger, J. Chem. Phys. **134**, 144302 (2011).
[18]D. B. Jones, S. M. Bellm, P. Limão-Vieira, and M. J. Brunger, Chem. Phys. Lett. **535**, 30 (2012).
[19]D. B. Jones, S. M. Bellm, F. Blanco, M. Fuss, G. García, P. Limão-Vieira, and M. J. Brunger, J. Chem. Phys. **137**, 074304 (2012).
[20]Z. Mašín, J. D. Gorfinkiel, D. B. Jones, S. M. Bellm, and M. J. Brunger, J. Chem. Phys. **136**, 144310 (2012).
[21]H. V. Duque, L. Chiari, D. B. Jones, P. A. Thorn, Z. Pettifer, G. B. da Silva, P. Limão-Vieira, D. Duflot, M.-J. Hubin-Franskin, J. Delwiche, F. Blanco, G. García, M. C. A. Lopes, K. Ratnavelu, R. D. White, and M. J. Brunger, Chem. Phys. Lett. **608**, 161 (2014).
[22]P. Limão-Vieira, D. Duflot, M.-J. Hubin-Franskin, J. Delwiche, S. V. Hoffmann, L. Chiari, D. B. Jones, M. J. Brunger, and M. C. A. Lopes, J. Phys. Chem. A **118**, 6425 (2014).
[23]L. Chiari, H. V. Duque, D. B. Jones, P. A. Thorn, Z. Pettifer, G. B. da Silva, P. Limão-Vieira, D. Duflot, M.-J. Hubin-Franskin, J. Delwiche, F. Blanco, G. García, M. C. A. Lopes, K. Ratnavelu, R. D. White, and M. J. Brunger, J. Chem. Phys. **141**, 024301 (2014).
[24]R. F. C. Neves, D. B. Jones, M. C. A. Lopes, K. L. Nixon, G. B. da Silva, H. V. Duque, E. M. de Oliveira, R. F. da Costa, M. T. do N. Varella, M. H. F. Bettega, M. A. P. Lima, K. Ratnavelu, G. García, and M. J. Brunger, J. Chem. Phys. **142**, 104305 (2015).
[25]R. F. C. Neves, D. B. Jones, M. C. A. Lopes, F. Blanco, G. García, K. Ratnavelu, and M. J. Brunger, J. Chem. Phys. **142**, 194305 (2015).
[26]*CRC Handbook of Chemistry and Physics*, 90th ed., edited by D. R. Lide (CRC Press, Boca Raton, FL, 2010).
[27]R. Rivelino, S. Canuto, and K. Coutinho, Braz. J. Phys. **34**, 84 (2004).
[28]T. Jewison, C. Knox, V. Neveu, Y. Djoumbou, A. C. Guo, J. Lee, P. Liu, R. Mandal, R. Krishnamurthy, I. Sinelnikov, M. Wilson, and D. S. Wishart, Nucleic Acids Res. **40**, D815 (2012).
[29]A. S. Mamman, J.-M. Lee, Y.-C. Kim, I. T. Hwang, N.-J. Park, Y. K. Hwang, J.-S. Chang, and J.-S. Hwang, Biofuels, Bioprod. Biorefin. **2**, 438 (2008).
[30]M. J. Brunger and P. J. O. Teubner, Phys. Rev. A **41**, 1413 (1990).
[31]L. Campbell, M. J. Brunger, P. J. O. Teubner, B. Mojarrabi, and D. C. Cartwright, Aust. J. Phys. **50**, 525 (1997).
[32]M. Allan, J. Phys. B **38**, 3655 (2005).
[33]H. Tanaka, M. J. Brunger, L. Campbell, H. Kato, M. Hoshino, and A. R. P. Rau, "Scaled plane-wave Born cross sections for atoms and molecules," Rev. Mod. Phys. (in press).
[34]R. F. da Costa, M. T. do N. Varella, M. H. F. Bettega, and M. A. P. Lima, Eur. Phys. J. D **69**, 159 (2015).
[35]M. J. Brunger and S. J. Buckman, Phys. Rep. **357**, 215 (2002).

[36]R. F. da Costa, E. M. de Oliveira, M. H. F. Bettega, M. T. do N. Varella, D. B. Jones, M. J. Brunger, F. Blanco, R. Colmenares, P. Limão-Vieira, G. García, and M. A. P. Lima, J. Chem. Phys. **142**, 104304 (2015).
[37]M. H. F. Bettega, L. G. Ferreira, and M. A. P. Lima, Phys. Rev. A **47**, 1111 (1993).
[38]R. F. da Costa, F. J. da Paixão, and M. A. P. Lima, J. Phys. B **37**, L129 (2004).
[39]J. S. dos Santos, R. F. da Costa, and M. T. do N. Varella, J. Chem. Phys. **136**, 084307 (2012).
[40]F. Blanco and G. García, Chem. Phys. Lett. **635**, 321 (2015).
[41]M. Hoshino, H. Murai, H. Kato, Y. Itikawa, M. J. Brunger, and H. Tanaka, Chem. Phys. Lett. **585**, 33 (2013).
[42]M. Hoshino, H. Murai, H. Kato, M. J. Brunger, Y. Itikawa, and H. Tanaka, J. Chem. Phys. **139**, 184301 (2013).